

Time-frequency based Coherence and Phase Locking Value Analysis of Human Locomotion Data using Generalized Morse Wavelets

Sopapun Suwansawang^{1,2} and David M. Halliday¹

¹*Department of Electronics, University of York, York, U.K.*

²*Department of Electronics, Faculty of Science and Technology, Nakhon Pathom Rajabhat University, Nakhon Pathom, Thailand*

Keywords: Analytic Wavelets, Phase Synchronization, Cone of Influence, Non-stationary Analysis.

Abstract: Time-frequency analysis is a powerful and popular tool for studying time-varying properties of non-stationary neurophysiological signals. In this study, time-frequency based coherence and phase locking value (PLV) analysis using generalized Morse wavelets are presented. The methods are applied to pairs of surface EMG signals recorded from leg muscles during treadmill walking in healthy human subjects. Time-frequency based coherence and PLV analysis in this study detect similar patterns of 8-15 Hz and 15-20 Hz common modulation of EMG during locomotion. Our results suggest that a combination of both methods would be suitable for investigating and characterising non-stationary neurophysiological data. An understanding of the basic principles of normal locomotion can further provide insight into pathological locomotion deficits.

1 INTRODUCTION

Human locomotion can be characterised by rhythmic activity that is governed by a series of complex interactions between the human brain and the spinal cord. These interactions can be analysed by recording electromyograms (EMG) from human muscles (Grosse et al., 2002; Halliday et al., 2003). An analysis of human movement is a process to investigate the characteristics of human body movement that relates to both normal and abnormal movement (Farmer et al., 2007; Tuncel et al., 2010). Understanding human movement or how the brain controls the muscles could help in recognising the first stages of many movement disorders, such as Parkinson's disease.

Analysis of the frequency content of electrophysiological signals are useful ways to examine neuronal synchrony (Grosse et al., 2002). Time-frequency analysis has been used extensively in studying time-varying properties of non-stationary neurophysiological signals (Tuncel et al., 2010; Allen and Mackinnon, 2010). Time-frequency coherence analysis is one of the methods used to represent signals whose frequency content is varying with time (Zhan et al., 2006). This analysis can be performed by mapping a one-dimensional signal in the time domain into a two dimensional

representation in time-frequency product space. Phase synchronisation is used to study phase relationships between physiological signals (Quyen et al., 2001; Lowet et al., 2016). Both time-frequency coherence and phase synchronisation analysis can be used to investigate and characterise non-stationary neuronal coupling mechanisms, and provided essentially the same information in frequency domain (Mezeiova and s, 2012). However, coherence analysis depends on two factors: phase consistency and amplitude covariation of signals (Quyen et al., 2001). Phase synchronisation analysis provides the phase component that can be obtained separately from the amplitude component for a given frequency or frequency range (Quyen et al., 2001).

The wavelet transform is increasingly applied in dynamic neurophysiological signal analysis in both time and frequency domain (Tuncel et al., 2010; Zhan et al., 2006; Quyen et al., 2001; Hassan et al., 2010). There are a number of wavelet families that are used in order to identify the appearance of oscillations and other signal properties. Currently, the continuous analytic wavelet transform is more widely used for the analysis of modulated oscillatory signals and discontinuities (Lilly and Olhede, 2010). The generalized Morse wavelets are exactly analytic wavelets that have been used to estimate characteristics of non-stationary

neurophysiological signals (Brittain et al., 2007; Nakhnikian et al., 2016). A particular subset of the generalized Morse wavelets, Airy wavelets, substantially outperforms the approximately analytic Morlet wavelets (Lilly and Olhede, 2010).

In this study, generalized Morse wavelets are applied to calculate time-frequency based coherence and phase locking value for ten experimental data sets: surface EMG during treadmill walking in healthy subjects. Our aim is to compare results from the two methods. The structure of the paper is organised as follows. First, we introduce the motivation and background of the study. Second, we provide a brief review of methodologies, with details about each of the required steps for their implementation. Third, we provide the detail of experiment data. Fourth, we illustrate the results of the experiment data. Fifth, we discuss our results in light of previous findings. The paper ends with suggestions for future work.

2 METHODS

This section provides details of analytical methods analysing non-stationary physiological signals. Section 2.1 describes generalized Morse wavelets, section 2.2 considers edge effects, section 2.3 gives a summary on the time-frequency coherence estimates, and section 2.4 presents the concepts of phase synchronisation analysis.

2.1 The generalized Morse Wavelets

Generalized Morse wavelets are a promising class of complex-valued exactly analytic wavelet transform with vanishing support on negative frequency axis, while the popular Morlet wavelet is only approximately analytic wavelet for sufficiently large radian frequency (Lilly and Olhede, 2009).

Generalized Morse wavelets are highly flexible and form a two-parameter family of wavelets. A definition of zero-order ($k = 0$) generalized Morse wavelets in the frequency domain form is provided in (Olhede and Walden, 2003) as

$$\Psi_{\beta,\gamma}(\omega) = \sqrt{2}H(\omega)A_{k;\beta,\gamma}\omega^\beta e^{-\omega^\gamma} \quad (1)$$

where $H(\omega)$ is the Heaviside unit step function and $A_{k;\beta,\gamma}$ is a normalising constant that can be expressed by

$$A_{k;\beta,\gamma} = \sqrt{\pi\gamma 2^r \Gamma(k+1)/\Gamma(k+r)} \quad (2)$$

where $\Gamma(\bullet)$ denotes the gamma function and $r = (2\beta + 1)/\gamma$. The maximum amplitude occurs at the peak frequency (Lilly and Olhede, 2009),

$$\omega_{\beta,\gamma} \equiv \left(\frac{\beta}{\gamma}\right)^{\frac{1}{\gamma}} \quad (3)$$

The rescaled second derivative of the frequency-domain wavelets evaluated at its peak frequency is $P_{\beta,\gamma}^2 \equiv \beta\gamma$, and $P_{\beta,\gamma}$ is called the dimensionless wavelet duration (Lilly and Olhede, 2010), defined as

$$P_{\beta,\gamma} \equiv \sqrt{\beta\gamma} \quad (4)$$

The time domain form for the generalized Morse wavelets may be expressed by the inverse Fourier transform,

$$\Psi_{\beta,\gamma}(t) = \frac{1}{2\pi} \int_0^\infty \sqrt{2}A_{k;\beta,\gamma}\omega^\beta e^{-\omega^\gamma} e^{i\omega t} d\omega \quad (5)$$

β and γ are two parameters controlling time-frequency localisation. The parameter β controls the time-domain decay, and γ controls the frequency-domain decay. Normally, β and γ are greater than zero. An example of one member of the generalized Morse wavelet family, the $\gamma = 3$ family with $\beta = 3, 9$, and 27 is shown in Figure 1. The $\gamma = 3$, called Airy wavelet, was found to have zero asymmetry in time domain and is nearly symmetric in the frequency domain. The Airy wavelets not only preserve the spirit of the Morlet wavelet but also substantially outperform the Morlet for high time localisation while remaining analytic. More details regarding the different roles of β and γ in controlling wavelet properties can be found in (Lilly and Olhede, 2009), (Lilly and Olhede, 2012), and (Lilly and Olhede, 2010).

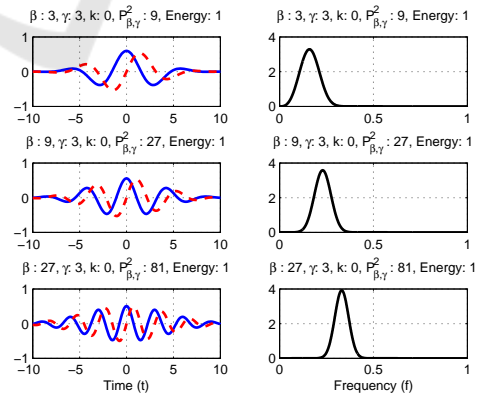


Figure 1: Examples of the generalized Morse wavelet for $\gamma = 3$ and $\beta = 3, 9$, and 27 , with time domain form $\Psi_{\beta,\gamma}(t)$ (left) and frequency domain form $\Psi_{\beta,\gamma}(\omega)$ (right). In the time domain, the solid line and the dashed line indicate the real part and the imaginary part of the wavelet, respectively. Frequency f is in cycles per second (Hz).

2.2 Cone of Influence

In practice, wavelet analysis is the convolution of the signal and the wavelet function, therefore the convolution will suffer edge effects. The region of a wavelet transform affected by edge effects is called the cone-of-influence (COI). Regions outside the COI are neglected due to edge effects. In this paper, the definition for identifying the COI is adapted from (Torrence and Compo, 1998). The COI for the Morlet wavelet is defined by the e-folding time $\tau_s = \sqrt{2}s$ which is chosen such that the wavelet power for a discontinuity at the edge drops by factor e^{-2} . To map this approach to the generalized Morse wavelet, the e-folding time at scale s can be defined as

$$\tau'_s = \sqrt{2}s \frac{P_{\beta,\gamma}}{\omega_{\beta,\gamma}} \quad (6)$$

where $P_{\beta,\gamma}$ and $\omega_{\beta,\gamma}$ refer back to (4) and (3), respectively. The e-folding time τ'_s will be used to visualize the COI in time-frequency plots of the wavelet power spectra, wavelet coherence and phase locking value.

2.3 The Estimation of Time-frequency Coherence

The analysis of time-frequency coherence requires the estimates for cross spectrum and auto spectra of two non-stationary processes. Considering two signals $x(t)$ and $y(t)$, the continuous wavelet transform expressions of their time-frequency representations are $W_x(\tau, f)$ and $W_y(\tau, f)$. The time-frequency cross spectrum between $x(t)$ and $y(t)$ signals is defined as

$$S_{xy}(\tau, f) = W_x(\tau, f)W_y^*(\tau, f) \quad (7)$$

and the time-frequency auto spectra of $x(t)$ and $y(t)$ signals are given as

$$S_x(\tau, f) = |W_x(\tau, f)|^2 \quad (8)$$

$$S_y(\tau, f) = |W_y(\tau, f)|^2 \quad (9)$$

The time-frequency coherence expression is obtained from equations (7), (8) and (9), the squared coherence can be calculated by the squared magnitude of the cross spectrum normalised by the auto spectra of each signal, is given by

$$|R_{xy}(\tau, f)|^2 = \frac{|S_{xy}(\tau, f)|^2}{S_x(\tau, f)S_y(\tau, f)} \quad (10)$$

In real situations, the auto-and cross-spectra can be estimated for a series of repeat trials that is computed by averaging across trials without smoothing within trials (Zhan et al., 2006). The

procedure for estimating the time-frequency coherence is outlined in equations (11)-(14), see (Zhan et al., 2006) for details. The time-frequency coherence is estimated from the cross spectrum $\hat{S}_{xy}(\tau, f)$ and the auto spectra $\hat{S}_x(\tau, f)$, and $\hat{S}_y(\tau, f)$ as

$$|\hat{R}_{xy}(\tau, f)|^2 = \frac{|\hat{S}_{xy}(\tau, f)|^2}{\hat{S}_x(\tau, f)\hat{S}_y(\tau, f)} \quad (11)$$

where

$$\hat{S}_x(\tau, f) = \frac{1}{N} \sum_{n=1}^N |W_n^x(\tau, f)|^2 \quad (12)$$

$$\hat{S}_y(\tau, f) = \frac{1}{N} \sum_{n=1}^N |W_n^y(\tau, f)|^2 \quad (13)$$

$$\hat{S}_{xy}(\tau, f) = \frac{1}{N} \sum_{n=1}^N W_n^x(\tau, f)W_n^{y*}(\tau, f) \quad (14)$$

where N is number of trials. Some assumptions are required of data in order to formulate a confidence interval for coherence estimates. This is essential for determining which values of coherence are reliable. The confidence interval means that the obtained coherence value can be viewed as significant if the estimated coherence value exceeds the confidence interval. If the two signals are independent and have Gaussian distributions, the distribution of the coherence estimates is given by (Gish and Cochran, 1988)

$$Pr(R^2 \leq r) = 1 - (1-r)^{(K-1)}, 0 \leq r \leq 1 \quad (15)$$

where $Pr(\cdot)$ denotes probability distribution function, r is the detection threshold value and K is the number of windows used to estimate the spectrum. For the confidence interval value of 95%, the detection threshold value for this confidence interval is computed as $r_{95\%} = 1 - 0.05^{1/(K-1)}$ (Zhan et al., 2006).

2.4 Phase Synchronisation Analysis

Phase synchronisation measures can be used to study the relationships between the phases of physiological signals. Phase synchronisation refers to the phases of two coupled oscillators that synchronise even if the amplitude fluctuations between the oscillating signals are uncorrelated (Pereda et al., 2005). Synchronisation of weakly coupled oscillating system appears as some relation between their phase and frequencies (Rosenblum and Kurths, 1998). A general framework for studying phase synchronisation has three main steps (Quyen and Bragin, 2007): first, pre-filtering of the raw signal with a bandpass filter around a chosen frequency value. Second, estimation of the phase. Third,

quantification of the degree of phase-locking. There are two methods of phase estimation, one using complex wavelets (Quyen et al., 2001; Lachaux et al., 1999) (refer back to (1) and another using the Hilbert transform (HT) (Tass et al., 1998). The main difference between these two methods is that the HT is actually a filter with unit gain at every frequency. If the signal is broadband, pre-filtering in the frequency band of interest is required before applying the HT, in order to get an appropriate phase value (Pereda et al., 2005). On the other hand, pre-filtering is unnecessary when using a complex wavelet because it can act as a bandpass filter and, at the same time, provide separate values for the instantaneous amplitude and the phase (Hassan et al., 2010). In this study, phase synchronisation is calculated using generalized Morse wavelets.

2.4.1 Phase Locking Value

Phase locking value (PLV) is an important measure for investigating synchronisation of neural activity, including the muscle activities detected by EMG. In particular, (Tass et al., 1998) found that the phase locking between the activity of primary and secondary motor areas can be related to the coordination of antagonistic muscles.

Analytically, the interaction between two oscillating systems essentially affects the evolution of their phases if the frequency ω_x and ω_y are in resonance for some integers p, q , indicating the ratios of possible frequency locking (for details see (Wacker and Witte, 2011) and (Tass et al., 1998)). The existence of locking or entrainment between frequencies are close to rational relation, $p\omega_x \approx q\omega_y$ (Pereda et al., 2005). The generalised phase difference of two series is given by

$$\varphi_{p,q}(t) = p\phi_x(t) - q\phi_y(t) \quad (16)$$

where $\phi_x(t)$ and $\phi_y(t)$ are the unwrapped phases of the signals. The principle of phase synchronisation of periodic self-oscillatory systems corresponds to a phase locking between two systems defined as

$$\varphi_{p,q}(t) = |p\phi_x(t) - q\phi_y(t)| \leq \text{constant} \quad (17)$$

Here, as the aim is to detect functional connectivity between two signals from the same physiological system. The m:n synchronisation index mostly considers the simplest case of $p = q = 1$. This is used here. The local phase of the generalized Morse wavelet transform for trial n at time τ and frequency f is quantified from the ratio between the imaginary part (\Im) and the real part (\Re) of the wavelet transform,

$$\phi_n^x(\tau, f) = \tan^{-1} \frac{\Im(W_n^x(\tau, f))}{\Re(W_n^x(\tau, f))} \quad (18)$$

The phase of a given time-series $x(t)$ can be defined such that it is parameterized in the range $\phi_n^x(\tau, f) \in [-\pi, \pi]$, with similar expressions for the phase of time-series y , $\phi_n^y(\tau, f)$. The phases are used to calculate the phase difference between $x(t)$ and $y(t)$ at time t . A representation of time-frequency phase locking values over N trials between the signals (Lachaux et al., 2000) is defined as

$$PLV(\tau, f) = \frac{1}{N} \left| \sum_{n=1}^N e^{i(\phi_n^y(\tau, f) - \phi_n^x(\tau, f))} \right| \quad (19)$$

PLV is a normalised measure that varies between 0 and 1, where a value of 1 means perfect phase synchrony.

2.4.2 The Statistical Significance Level of PLV

The statistical significance of phase locking values is determined by using surrogate series. These surrogate series are created by shifting the trials of signal y (see (Lachaux et al., 2000), (Pereda et al., 2005), and (Gupta and James, 2007) for details). In this study, the significance level for PLV is considered if the PLV is greater than the 95% confidence interval of the von Mises distribution of the mean of PLV calculated from surrogate data. The percentage of the linear Normal distribution ($z=1.96$) is used to give the 95% confidence interval for the mean direction in Von Mises distribution. The value of confidence limit depends on the number of trials. A small number of trials will result in a large confidence limit. In this study, for 380 trials, a PLV above 0.0538 is statistically significant at $P < 0.05$. For comparison the 95% significance level for coherence with 380 trials is 0.0079.

3 EXPERIMENTAL DATA

3.1 Data

Ten datasets were taken from the study of (Halliday et al., 2003), using experiments to investigate the functional coupling of motor units during treadmill walking in healthy subjects. All subjects were made to walk on a treadmill at normal speed. Paired surface EMG electrodes were placed over two sides from the ankle flexor TA. Surface EMG was used to record the aggregate muscle potentials (Mima et al., 2001). The two EMG signals over the ankle flexor can be used as a substitute for pairs of motor unit recordings that can identify any modulation in the functional coupling during walking, and provide a basis for investigating

the highly adaptive nature of human gait patterns (Halliday et al., 2003). Recordings were made over a period of 500 seconds. A contact switch identified heel strike. Thresholding of the heel strike record provides a sequence of trigger times. These trigger times provide a reference point within each step cycle which is used to segment the data for undertaking time-frequency analysis, where time is defined with respect to heel contact. Further details of experiments are given in (Halliday et al., 2003). Examples of EMG signals obtained from one subject during treadmill walking are in Figure 2.

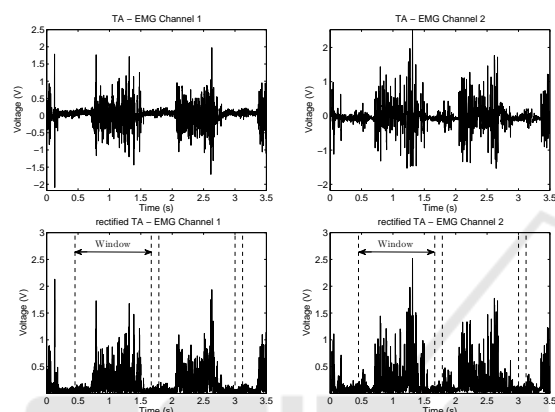


Figure 2: An example of paired surface EMG signals obtained from one subject during treadmill walking, with (top) the EMG signal before rectification and (bottom) rectified EMG signal showing analysis window.

3.2 Data Analysis

In this paper, the power spectrum, coherence and PLV were computed using generalized Morse wavelets with $\gamma = 3$ and $\beta = 9$. The aim is to investigate the functional coupling between paired EMG signals in the time-frequency domain. The standard practice of rectification of surface EMG signals has been a commonly used pre-processing procedure that allows detection of significant coherence (Farmer et al., 2007). EMG-EMG spectral and PLV analysis were calculated using averages over 380-step cycles. All steps were segmented into 1040 ms segments with 820 ms before heel trigger and 220 ms after heel trigger. The time scale on time-frequency plots is labelled as 0-1040 ms, heel triggers are at 820 ms in these plots (Figure 3). Thus, each coherence and PLV plot covers swing phase including early, mid, and late swing for each step cycle. Examples of rectified EMG signal and analysis window are provided in Figure 2. The EMG-EMG coherence and PLV was considered significant if above the 95% confidence limits, calculated using (15) for coherence and in

section 2.4.2 for PLV. Significant coherence and PLV were observed at frequencies ≤ 50 Hz. All analyses were implemented using MATLAB (The MathWorks, Natick, MA).

4 RESULTS

Examples of time-frequency power spectra, coherence and PLV from two subjects walking at 4 km/h are shown in Figure 3. Figure 3A and B illustrate estimates of spectra for each EMG channel. Figure 3C and D illustrate time-frequency coherence and PLV estimates between the EMG signals. Figure 3E and F illustrate line plots of the 8-to 15- and 15- to 20-Hz rhythmic components in coherence and PLV estimates averaged over these frequency ranges, respectively. Spectra are plotted as Log values. Only coherence and PLV inside the COI are represented on the line plots. The 95% confidence limit for coherence estimate in this study is 0.0079, and 0.0538 for PLV based on analysis of 380 step cycles. The black line indicates the COI in Figure 3A-D (see section 2.2).

Table 1: Summary of mean coherence and PLV from 380-step cycles for 10 subjects at frequency 2-50 Hz in beginning, middle and end swing of the step cycle.

| No. | Coherence | | | PLV | | |
|-----|-----------|------|------|-------|------|------|
| | Begin | Mid | End | Begin | Mid | End |
| 1 | 0.28 | 0.24 | 0.44 | 0.54 | 0.46 | 0.60 |
| 2 | 0.34 | 0.41 | 0.44 | 0.46 | 0.52 | 0.57 |
| 3 | 0.34 | 0.40 | 0.43 | 0.45 | 0.52 | 0.55 |
| 4 | 0.40 | 0.33 | 0.43 | 0.54 | 0.46 | 0.56 |
| 5 | 0.42 | 0.36 | 0.45 | 0.55 | 0.48 | 0.57 |
| 6 | 0.45 | 0.43 | 0.62 | 0.57 | 0.55 | 0.77 |
| 7 | 0.41 | 0.39 | 0.47 | 0.57 | 0.55 | 0.61 |
| 8 | 0.46 | 0.42 | 0.57 | 0.60 | 0.54 | 0.65 |
| 9 | 0.48 | 0.43 | 0.57 | 0.61 | 0.53 | 0.64 |
| 10 | 0.50 | 0.41 | 0.50 | 0.64 | 0.53 | 0.64 |

The results suggest that the wavelet spectra of EMG signals are similar over all subjects. There is an increase in power in early, with a reduction in the middle and then increase in late swing of the step cycle (Figure 3A and B). Strongest coherence is at frequency < 5 Hz. In some subjects this low frequency component persists across the swing phase (Figure 3D), in other subjects it is prominent in the early and late phases of swing (Figure 3C). Note that some of the low frequency coherence is outside the COI, therefore potential edge effects should be taken into account. In addition, weaker coherence between 8

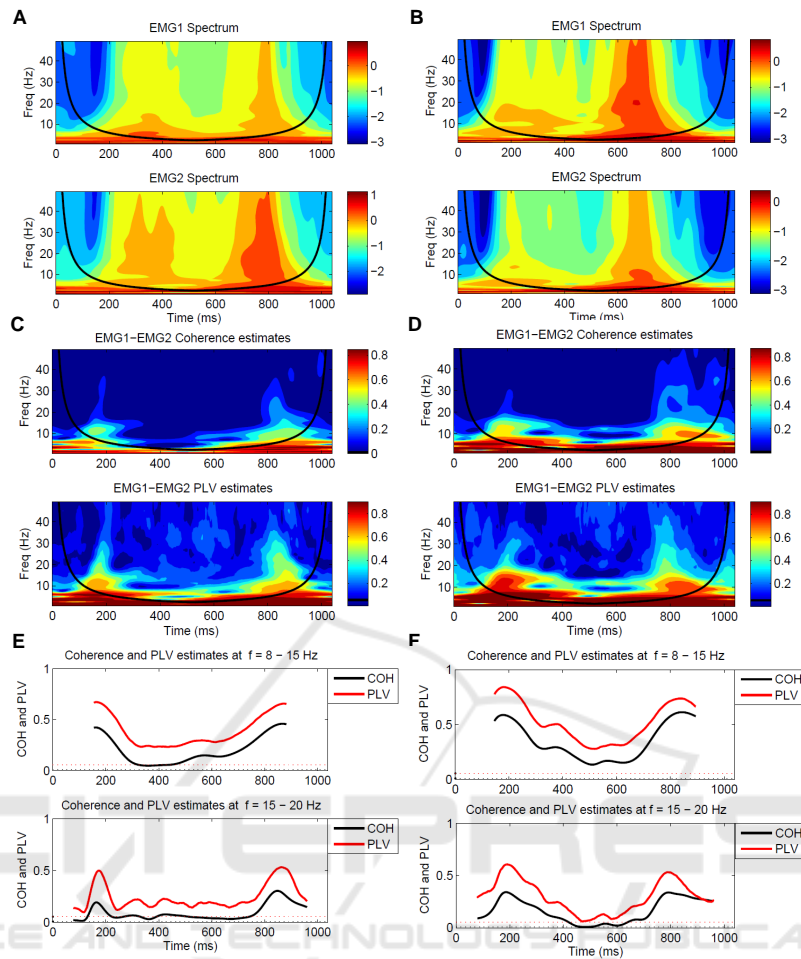


Figure 3: EMG-EMG wavelet coherence and PLV analysed from 380-step cycles, which segmented into 1040 ms non overlapping epochs from two subjects, subject 1 (left column) and subject 10 (right column). A and B: estimates of spectra for each EMG channel, C and D time-frequency coherence and PLV plots, E and F: line-plot of coherence and PLV estimates at $f = 8-15$ Hz, and $f = 15-20$ Hz. Two horizontal dashed lines in E and F are the 95% confident limit for coherence estimates (black) and PLV estimates (red).

and 20 Hz occurs in early and late swing. PLV has significant features in both time and frequency which are similar to those seen in coherence estimates; see Figure 3C-F.

Some aspects are common across all the experiments as illustrated in Table 1. The magnitude of the correlation between paired EMG signals is not constant over the step cycle. For 8 of the 10 subjects, the magnitude of the coherence and the PLV reduce during the mid swing of the step cycle. Two of the subjects (subjects 2 and 3) have magnitude in the early swing that is smaller when compared to mid and end swing. A significant low-frequency (< 8 Hz) component is present throughout the step cycle, but some of these features are outside the COI so many reflect edge effects in wavelet transform. A distinct 8- to 15- and 15- to 20-Hz correlation are present during

early and late swing as illustrated clearly in Figure 3E and F. Analysis of this locomotion data using wavelet coherence and wavelet PLV gives similar results.

5 DISCUSSION

This study presents time-frequency coherence and PLV analysis using generalized Morse wavelets with $\beta = 9$ and $\gamma = 3$. The methods are used to characterise the correlation structure in experimental data consisting of paired surface EMG signals during treadmill walking. The main finding of the study is that both methods are able to detect localised correlation in the time-frequency plane. The results obtained in this study are similar to Fourier based

time-frequency estimates in (Halliday et al., 2003), functional coupling of motor unit during locomotion was investigated. This demonstrated the presence of 8-15 Hz and 15-20 Hz, frequency components of motor unit correlation. These frequency components are prominent around heel contact, which reflect rhythmic neural activity associate with a particular phase of locomotion. Traditional spectral analysis method based on Fourier transform contains no temporal information. (Halliday et al., 2003) applied coherence function and estimates of the cumulant density function to characterise the correlation between the EMG signals in the frequency domain and the time domain, respectively. By analysing data, each step cycle was divided into three different non-overlapping segments each lasting 200 ms corresponding to early, mid, and end swing.

The generalized Morse wavelet based coherence and PLV estimates in this study provide a similar description of the data. The PLV estimates have larger magnitudes than the coherence estimates. The PLV appears noisier than the coherence despite the same number of trials (Figure 3C-D). The confidence limit derived from surrogate data is larger for the PLV estimate than for the coherence estimate for the same number of trials. The wavelet edge effects should not be a problem if the window length is made sufficiently large. For example, for a frequency of 10 Hz the edge effect has duration around 120 ms for the generalized Morse wavelets used here. Changes in parameters β and γ relate to temporal and spectral resolution in the time-frequency plane. Adjustment of these will alter the resolution in time and frequency (Lilly and Olhede, 2009).

Our results suggest both methods give useful information and are suitable for investigation of non-stationary neuronal coupling mechanisms underlying human treadmill locomotion. Although this study is constrained to EMG acquired during walking, this approach could be applied to other physiological data.

6 FUTURE WORK

The methods in this study will be used to identify modulations in the functional coupling of motor units during overground walking in normal and Parkinson's disease subjects. This will provide insight into the organisation of the neural pathways involved in gait patterns in health and disease.

ACKNOWLEDGEMENTS

Financial support is provided by the Royal Thai government science and technology scholarships.

REFERENCES

- Allen, D. P. and Mackinnon, C. D. (2010). Time-Frequency analysis of movement-related spectral power in EEG during repetitive movements: a comparison of methods. *Journal of Neuroscience methods*, 186:107–115.
- Brittain, J.-S. et al. (2007). Single-trial multiwavelet coherence in application to neurophysiological time serie. *IEEE Transactions on Biomedical Engineering*, 54(5):854–862.
- Farmer, S. F. et al. (2007). Changes in EMG coherence between long and short thumb abductor muscles during human development. *J Physiol*, 579:389–402.
- Gish, H. and Cochran, D. (1988). General coherence. *In: International Conference on Acoustic, Speech and Signal Processing*, 5:2745–2748.
- Grosse, P. et al. (2002). EEG-EMG, MEG-EMG and EMG-EMG frequency analysis: physiological principles and clinical applications. *Clinical Neurophysiology*, 113:1523–1531.
- Gupta, D. and James, C. J. (2007). Narrow band vs. broadband phase synchronization analysis applied to independent components of Ictal and Interictal EEG. *Proceeding of the 29th annual international conference of the IEEE EMBS Cite internationale*, pages 23–26.
- Halliday, D. M. et al. (2003). Functional coupling of motor units is modulated during walking in human subjects. *J Neurophysiol*, 89:960–968.
- Hassan, M. et al. (2010). Interactions between Uterine EMG at different sites investigated using wavelet analysis: comparison of pregnancy and labor contraction. *EURASIP J. Adv. Signal Process*, 17:1–9.
- Lachaux, J. P. et al. (1999). Measuring phase synchrony in brain signals. *Hum. Brain Mapp.*, 8:194–208.
- Lachaux, J. P. et al. (2000). Studying single-trials of phase synchronous activity in the brain. *International Journal of Bifurcation and Chaos*, 10(10):2429–2439.
- Lilly, J. M. and Olhede, S. C. (2009). High-order properties of analytic wavelets. *IEEE Transactions on Signal Processing*, 57:146–160.
- Lilly, J. M. and Olhede, S. C. (2010). On the analytic wavelet transform. *IEEE Transactions on Information Theory*, 56:4135–4156.
- Lilly, J. M. and Olhede, S. C. (2012). Generalized morse wavelet as a superfamily of analytic wavelets. *IEEE Transactions on Signal Processing*, 60(11):6036–6041.
- Lowet, E. et al. (2016). Quantifying neural oscillatory synchronization: a comparison between spectral coherence and phase-locking value approaches. *PLOS one*, 11(1):1–37.

- Mezeiová, K. and s, M. P. (2012). Comparison of coherence and phase synchronization of the human sleep electroencephalogram. *Journal of Clinical Neurophysiology*, 123(9):1821–1830.
- Mima, T. et al. (2001). Coherence between cortical and muscular activities after subcortical stroke. *Stroke*, 32(11):2597–2601.
- Nakhnikian, A. et al. (2016). A novel cross-frequency coupling detection method using the generalized morse wavelet. *Journal of Neuroscience Methods*, 269:61–73.
- Olhede, S. C. and Walden, A. T. (2003). Polarization phase relationships via multiple morse wavelet. I fundamentals. *Proc. Roy. Soc. Lond*, 60(11):6036–6041.
- Pereda, E. et al. (2005). Nonlinear multivariate analysis of neuroohysiological signals. *Prog Neurobiol*, 77:1–37.
- Quyen, M. L. V. and Bragin, A. (2007). Analysis of dynamic brain oscillations: methodological advances. *Trends Neurosci*, 30(7):365–373.
- Quyen, M. L. V. et al. (2001). Comparision of hilbert transform and wavelet methods for the analysis of neuronal synchrony. *Journal of neuroscience methods*, 111:83–98.
- Rosenblum, M. G. and Kurths, J. (1998). Analysing synchronisation phenomena from bivariate data by means of the hilbert transform. In: *Nonlinear Analysis of Physiological data*, pages 91–99.
- Tass, P. et al. (1998). Detection of n:m phase locking from noisy data: Application to magnetoencephalography. *Phys. Rev. Lett.*, 81:3291–3294.
- Torrence, C. and Compo, G. P. (1998). A practical guide to wavelet analysis. *Bulletin of the American Meteorological Society*, 76:61–78.
- Tuncel, D. et al. (2010). Time Frequency based coherence analysis between EEG and EMG activities in fatigue duration. *Journal of Medical Systems*, 34(2):131–138.
- Wacker, M. and Witte, H. (2011). On the stability of the n:m phase synchronization index. *IEEE Transactions on Biomedical Engineering*, 58(2):332–338.
- Zhan, Y. et al. (2006). Detecting time-dependent coherence between non-stationary electrophysiological signal-a combined statistical and time-frequency approach. *Journal of neuroscience methods*, 156:322–332.